NANOSYSTEMS:
PHYSICS, CHEMISTRY, MATHEMATICS

Original article

Sumina A.A.. et al. *Nanosystems: Phys. Chem. Math.*, 2025, **16** (1), 105–115.
http://nanojournal.ifmo.ru
DOI 10.17586/2220-8054-2025-16-1-105-115

Nickel-copper-containing alloy catalysts for furfural hydroconversion: the influence of composition and physicochemical features on the distribution of reaction products in various modes

Anastasiya A. Sumina[a], Svetlana A. Selishcheva[b], Olga A. Bulavchenko[c], Vadim A. Yakovlev[d]

Federal Research Center Boreskov Institute of Catalysis SB RAS, Novosibirsk, Russia

[a]sumina@catalysis.ru, [b]svetlana@catalysis.ru, [c]obulavchenko@catalysis.ru, [d]yakovlev@catalysis.ru

Corresponding author: Svetlana A. Selishcheva, svetlana@catalysis.ru

PACS 82.45.Jn

ABSTRACT In this work, nickel-copper-containing alloy catalysts with different contents of nickel oxide were prepared and used in the furfural hydroconversion to 2-methylfuran and furfuryl alcohol. The most active catalyst (7Ni19Cu61Fe13Al) was chosen. We selected the reaction conditions, providing a high yield of 2-methylfuran (81 wt. %) at 100 % furfural conversion in a batch reactor: $T = 200$ °C, $P(H_2) = 5.0$ MPa, reaction time 4 h. The selected catalyst was studied by a complex of physicochemical methods; we determined the phase and surface composition, the morphology of the active component, and the possible cause of catalyst deactivation during the reaction due to the irreversible sorption of reactants and reaction products, as well as their polymeric structures on the catalyst surface. We have demonstrated the possibility of obtaining 2-methylfuran for the 7Ni19Cu61Fe13Al catalyst with a selectivity of 70 % at 87 % conversion of furfural in a flow-type reactor without solvent at $LHSV = 6$ h^{-1}, $T = 200$ °C, $P(H_2) = 5.0$ MPa.

KEYWORDS hydroconversion, furfural, catalysis, value-added chemicals, batch reactor, flow-type reactor

ACKNOWLEDGEMENTS The work was supported by the Ministry of Science and Higher Education of the Russian Federation within the governmental order for Boreskov Institute of Catalysis (project FWUR-2024-0043).

FOR CITATION Sumina A.A.. Selishcheva S.A.. Bulavchenko O.A.. Yakovlev V.A. Nickel-copper-containing alloy catalysts for furfural hydroconversion: the influence of composition and physicochemical features on the distribution of reaction products in various modes. *Nanosystems: Phys. Chem. Math.*, 2025, **16** (1), 105–115.

1. Introduction

Currently, due to the depletion of fossil resources, there is an increasing relevance in the search for new alternative sources used to produce raw materials. One of the sources for obtaining valuable chemical compounds are hemicelluloses, which are extracted during the processing of plant materials [1]. Hemicelluloses are of particular interest to the industry due to their low content of heavy metals, sulfur, and nitrogen, making them safer to process.

Furfural is obtained through the acid hydrolysis of hemicelluloses (Fig. 1a), and its world production in 2021 exceeded 300,000 tons [2]. Furfural is a platform for the synthesis of various chemicals due to its reactive aldehyde groups and conjugated double bonds [3]. Furfural derivatives are widely used to produce organic solvents, pharmaceuticals, agrochemicals, perfumes, biofuels, fuel additives, and synthetic resins or rubber [4]. One of the most interesting and common methods for processing furfural is hydroconversion, as the products obtained have a high value added [5]. For example, 2-methylfuran (2-MF), which is used in the fuel industry as an octane-boosting additive due to its high octane number (101) [6], as well as in medicine and pharmaceuticals as a precursor in the production of dietary supplements and drugs. The hydroconversion of furfural to 2-MF can proceed in two ways: through the intermediate formation of furfuryl alcohol (FA) or directly through the hydrogenolysis of the C=O double bond (Fig. 1b) [7, 8].

Traditional catalysts for the furfural hydroconversion to target products (2-MF, FA) are high-percentage copper-chromium ones [10], as well as catalysts based on noble metals [11, 12]. However, despite their high activity, these systems have several disadvantages. Use of chromium catalysts can contribute to toxic emissions due to the tendency of Cr^{6+} compounds to dissolve in many organic and inorganic solvents, including furfural [13, 14]. During the catalyst preparation stage, substances containing Cr^{6+} are used, and Cr^{6+} is also present in the fresh oxide catalyst (for example, in the following compounds: $CuCrO_4$, $CuCrO_4{\cdot}Cu(OH)_2$, $2CuCrO_4 \cdot 3Cu(OH)_2{\cdot}H_2O$) [15, 16]. During preliminary calcination or reduction in the preparation stage, the transition of chromium from the $+6$ state to the $+3$ state may be incomplete, which subsequently leads to contamination of the target products. Additionally, in some cases, these catalysts deactivate quickly, necessitating the use of high hydrogen pressure. In the case of noble metal catalysts, the primary limiting factor is their high cost [17].

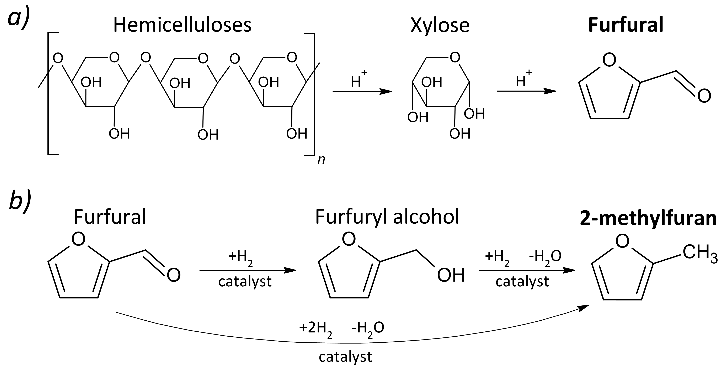

FIG. 1. a) The scheme for obtaining furfural from hemicelluloses [9]; b) The scheme of furfural hydroconversion over catalysts

Transition-based chromium-free systems can act as an alternative to the above-mentioned catalysts. Copper is one of the most active metals in the hydroprocessing of organic substances, particularly in the conversion of furfural into various C5-C6 organic compounds [18, 19]. Yunlong Yao et al. found that the Zn-modified Cu-containing catalyst demonstrated good results in the hydrogenation of furfural (100 % conversion) to FA ($\sim$ 100 % yield) under the following reaction conditions: 120 °C, 2.0 MPa, 0.2 g catalyst, 100 mL/min H_2, WHSV 0.3 h^{-1}) [20]. However, such systems are not suitable for obtaining 2-MF with high selectivity.

Doping of copper systems with nickel and cobalt accelerates furfural conversion and increases 2-MF yield [21, 22]. Munsuree Kalong et al. [23] describe monometallic copper samples supported on alumina, as well as the systems doped with nickel and cobalt. The conversion of furfural in the batch reactor reached 100 % of all samples over a reaction time of 2 hours. However, the nickel-promoted catalyst proved to be the most efficient. The maximum 2-MF yield obtained was 47 – 50 % at a reaction time of 2 hours. The authors concluded that doping with nickel enhances the activity of the catalyst and accelerates the reaction rate. In the work [24], the authors studied Ni–Fe catalysts obtained by co-precipitation; a 2-MF yield of up to 80 % was achieved, with complete conversion of furfural and a reaction time of 10 hours in the batch reactor over the catalyst. Apparently, high yields were due to the presence of fine metallic nickel particles and strong acid sites on the catalyst surface, represented by metal oxides, which promote the activation of the aldehyde group and the reduction of the C=O bond. Acidic sites on iron oxide are often employed to activate oxygen in molecules of aldehydes, acids, and alcohols [25], as well as in the Fischer–Tropsch process for the adsorption and activation of carbon monoxide molecules [26].

It should be noted that the high content of transition metals promotes the hydrogenation of the furan ring, resulting in the formation of tetrahydrofurfuryl alcohol (THFA), 1-pentanol, pentanal, 2-methyltetrahydrofuran (2-MTHF), etc. [27, 28]. However, at low concentrations, such additives enable the successful hydrogenation of the aldehyde group of furfural while preserving the structure of the furan ring [29].

The work [30] examined CuFeAl catalysts, which were prepared by the fusion method. Metallic copper serves as the active component of such systems. The modifying additives of aluminum and iron form a matrix for the active component, promote the formation of fine particles of copper, prevent its sintering, and prolong the service life of the catalyst. Nevertheless, this system is effective to produce FA; a higher content of a more active component is necessary in the catalyst to obtain 2-MF. The addition of nickel to the composition of such a system can improve the 2-MF selectivity. Previously, NiCu-containing catalysts were studied in the hydroconversion processes of bio-oil [31], as well as in its model compounds (anisole, guaiacol) [32], and in the hydrotreatment of vegetable oils [33].

In this work, we considered high-percentage NiCu-containing alloy catalysts with different contents of nickel oxide (5 – 10 wt.%) for the hydroconversion of furfural into FA and 2-MF. We tested the obtained catalysts in both a batch reactor with diluted feedstock and a flow-type reactor with pure furfural. The first method is well-studied and found in many works; however, the second method is less commonly used but more applicable for transition to industrial conditions. We studied the physicochemical properties of such systems and selected the optimal metal content in the catalyst to ensure maximum selectivity for the desired product (2-MF).

2. Experimental

We used the salt fusion method for the preparation of catalysts for the hydroconversion of furfural. We mixed the calculated weights of aqueous nitrates of iron, aluminum, copper, and nickel in a quartz bowl and heated on an electric stove to $\sim$ 300 °C. Next, the catalyst was calcined in a muffle furnace at a temperature of 450 °C for an hour. As a result, three catalysts were obtained: 5Ni19Cu63Fe13Al (5Ni), 7Ni19Cu61Fe13Al (7Ni), and 10Ni18Cu60Fe12Al (10Ni); value indicates metal oxide content (wt. %) in the sample.

The study of samples of the H_2-TPR method was carried out on a Chemosorb device (JSC Modern Laboratory Equipment, Moscow, Russia).

The XRD, in situ XRD, XPS, HRTEM, CHNS methods, textural characteristics of the reduced catalysts, the amount of chemisorbed CO on reduced catalysts at 250 °C, and qualitative and quantitative analysis of liquid products were previously described in [19].

Furfural (GOST 10930-74) was used for hydroconversion experiments and was pre-purified in a vacuum distillation unit. Isopropyl alcohol (GOST 9805-84) was used as a solvent to carry out the process in a batch reactor.

The furfural hydroconversion was carried out in a batch reactor with a volume of 300 cm^3. The reactor is equipped with a mechanical stirrer with a magnetic drive, a thermocouple, and a pressure sensor, as well as a control system for stirring speed, temperature, and pressure. Reduction conditions: $T = 250$ °C, hydrogen flow = 100 ml/min, $t = 1$ h; reaction conditions: $P(H_2) = 5$ MPa, mixing speed = 1800 rpm, $T = 160 - 250$ °C, $t = 4$ h.

The furfural hydroconversion in a flow-type unit was carried out using a reactor with a volume of 10 cm^3, into which we placed a catalyst weighing 1 g (fraction size 0.25 – 0.50 mm) mixed with quartz in a volume ratio of 1:4. We used crystalline purified quartz with a fraction size of 0.25 – 0.50 mm. Reduction conditions: $T = 250$ °C, hydrogen flow = 100 ml/min, $t = 1$ h; reaction conditions: $P(H_2) = 5$ MPa, $T = 200$ °C, LHSV = $1 - 8$ h^{-1}.

The thermal analysis was carried out using an STA 449 C Jupiter synchronous thermal analysis instrument from NETZSCH (Selb, Germany). For the study, the sample was placed in a crucible corundum. The rate of air supply to the sample chamber was 30 ml/min. The sample was heated at a rate of 10 °C/min to 1000 °C. The experimental data were analyzed using the NETZSCH Proteus Thermal Analysis software package (Selb, Germany).

3. Results and discussion

3.1. Characterization of fresh catalysts

We determined the reduction temperature of the obtained fresh catalysts using temperature-programmed reduction with hydrogen (H_2-TPR). The results showed that there are two regions of hydrogen uptake for all samples (Fig. 2). The first region is in the low-temperature range (200 – 330 °C), where copper and nickel oxide particles are reduced. The second region is in the high-temperature range (500 – 850 °C), where iron oxide is gradually reduced to metal.

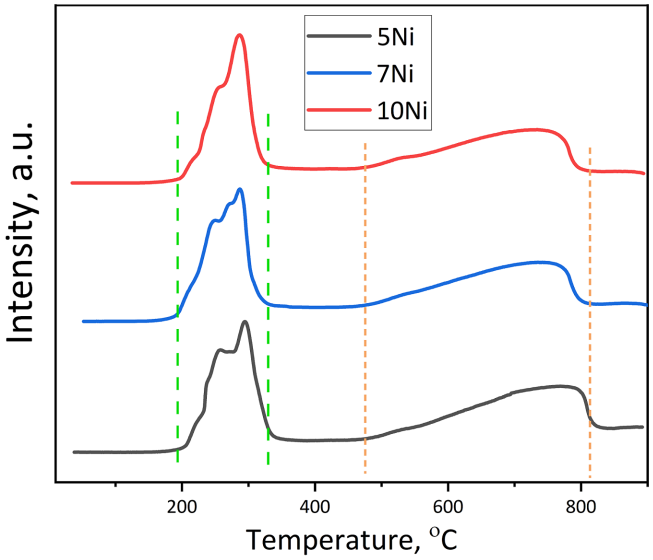

FIG. 2. H_2-TPR profiles of studied catalysts

Based on the data obtained from the H_2-TPR analysis, we chose a reduction temperature of 250 °C, which would reduce fine copper and nickel oxides.

The study of unreduced catalysts to determine their phase composition was carried out using X-ray diffraction analysis (XRD). For three catalyst samples (5Ni, 7Ni, and 10Ni) the X-ray patterns are similar (Fig. 3). The main peaks correspond to reflections from hematite (Fe_2O_3), and the CuO reflection is also observed (the peak with a maximum at $2\theta = 38.8°$ corresponds to the CuO reflection [111]). In the domain $2\theta = 35 - 37°$, there is a superposition of reflections [110] and [11-1] of CuO and [110] of Fe_2O_3. The absence of reflections corresponding to NiO and Al_2O_3 can be explained by their X-ray amorphous state.

The composition of the catalyst surface layer was studied using X-ray photoelectron spectroscopy (XPS). We examined three catalyst samples (5Ni, 7Ni, and 10Ni) after reduction at 250 °C.

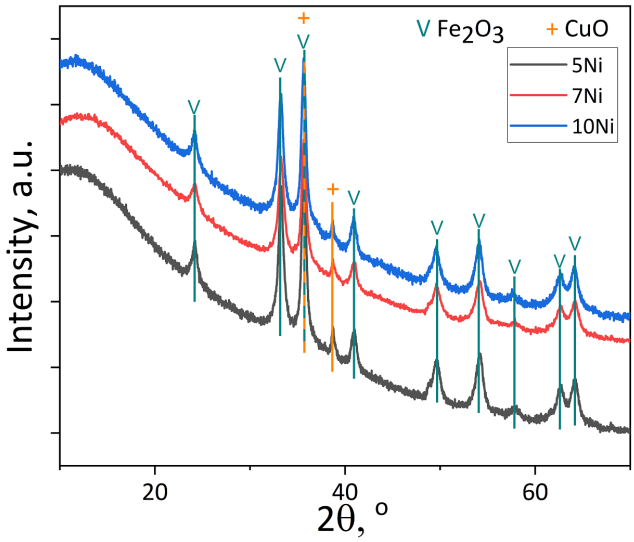

FIG. 3. X-ray patterns of unreduced catalysts

Figure 4a shows the Ni2p spectra of the studied catalysts. In the Ni2p spectra, we observed a reverse orbital splitting, and two groups of peaks associated with the $Ni2p_{3/2}$ and $Ni2p_{1/2}$ levels. In the spectra of the studied catalysts, a peak for the $Ni2p_{3/2}$ bond was found in the region of 852.8 eV, along with a peak for plasma losses in the region of 858.9 eV. Additionally, the presence of a peak in the region of 855.3 eV, accompanied by "main" satellite peaks in the regions of 857.1 and 862.0 eV, is typical for Ni^{2+} compounds. Thus, after reduction treatment, a portion of the nickel is in the metallic state (38 – 43 %), while the remainder is in the Ni^{2+} state as nickel oxide (NiO) [34, 35].

Figure 4b presents the spectra of the Cu2p catalysts. We observe back-orbital splitting, and two groups of peaks associated with the levels of $Cu2p_{3/2}$ (in the regions of 932.6 and 946.0 – 949.3 eV) and $Cu2p_{1/2}$. The shape of the spectra allows us to assert that almost all copper in the near-surface layer of the catalyst is in the reduced state [36–38].

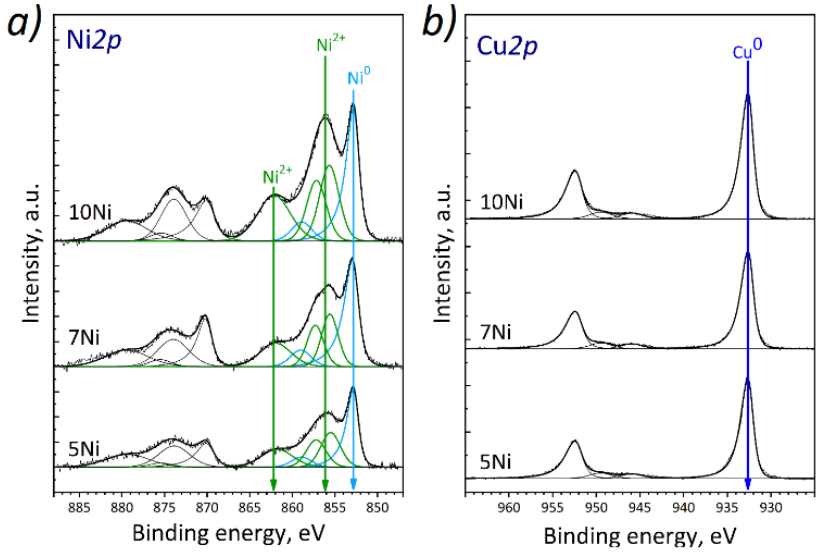

FIG. 4. Spectra a) Ni2p; b) Cu2p of the studied catalysts

According to XPS data, aluminum is completely in the oxide form (Al_2O_3). Furthermore, it was found that iron is predominantly in the Fe^{3+}/Fe^{2+} state, which likely corresponds to partially reduced iron oxide (Fe_3O_4), in which most of the iron cations are in the Fe^{2+} state [39, 40].

To determine the textural characteristics of the catalysts, we employed N_2 physical adsorption (BET) and CO chemisorption methods. Table 1 presents the results of the study on the fresh samples in oxide form and reduced catalysts. It should be noted that the textural characteristics of the samples determined by using the BET method are practically identical. However, based on the CO chemisorption data for pre-reduced samples (at 250 °C), it can be inferred that the catalyst with 7 wt.% nickel oxide content may exhibit higher activity in the target process compared to the other samples. Apparently, in this case, the optimal Cu/Ni ratio is achieved, which promotes the formation of a larger number of

active centers on the catalyst surface. Nickel doping of the 20Cu66Fe14Al catalyst increased the amount of adsorbed CO from 31 μmol/g_{cat} [30] to 85 μmol/g_{cat}. Thus, we can assume that the main adsorption centers for the 7Ni sample are predominantly nickel particles.

TABLE 1. Textural characteristics of catalysts in oxide[1] and reduced[2] forms

Catalyst	A^1_{BET}, m^2/g	$V_{pore\Sigma}{}^1$, cm^3/g	Amount of adsorbed CO[2], μmol/g
5Ni	50	0.11	58
7Ni	55	0.10	85
10Ni	53	0.11	49

The data obtained from the H_2-TPR and CO chemisorption methods correlate with each other: the optimal reduction temperature for the catalysts is 250 °C, at which finely dispersed nickel oxide particles transition to a metallic state and copper oxide is completely reduced.

3.2. Catalytic performance in a batch reactor

To compare the obtained catalysts, we studied them during the hydrogenation of furfural in a batch reactor and established correlations between the product composition, reaction temperature, catalyst composition, and mass of the loaded catalyst.

FA is the main product for the 5Ni catalyst; its weight content at low temperatures (160 °C) is 98 % (Fig. 5a). As the temperature rises (200 – 250 °C), 2-MF begins to form, with a maximum yield of 32 % at 250 °C. In addition, under these conditions, small quantities of by-products (2-MTHF and THFA) are formed (4 wt.%) (Fig. 5a).

The formation of 2-MF requires more stringent hydrogenation conditions, such as the presence of a catalyst with a higher nickel oxide weight content. Over the 7Ni catalyst, the hydrogenation of furfural is faster compared to the 5Ni catalyst; at 200 °C, the yield of 2-MF increases to 20 %, though by-products (THFA and 2-MTHF) are also formed. At higher reaction temperatures (250 °C), the content of the target product (2-MF) increases to 67 %.

Further, increases in the mass content of nickel oxide in the catalyst lead to greater formation of by-products. For example, over the 10Ni catalyst at 200 °C, the yield of by-products (THFA and 2-MTHF) doubles compared to the 7Ni sample. As the reaction temperature rises to 250 °C, the yield of 2-MF decreases to 48 %, while the yield of FA almost doubles (from 23 to 40 %).

The data obtained for the hydroconversion of furfural correlate with the CO chemisorption results: the most active catalyst in the target process is 7Ni.

Based on the dependencies obtained, we selected the reaction conditions to achieve 100 % selectivity for FA under relatively mild conditions (H_2 5.0 MPa, 160 °C, mass of 7Ni catalyst is 0.3 g, reaction time 4 h). Additionally, we determined that the optimal temperature for the hydroconversion of furfural to 2-MF is 200 °C.

To increase the yield of the desired product (2-MF) at this temperature, we increased the catalyst loading to 1 g.

Comparing the three catalysts (Fig. 5b), we observed a greater reaction depth for the sample with a nickel oxide mass content of 7 %. 2-MF was obtained in high yield, with relatively low concentrations of side products. The 7Ni catalyst was chosen for further study, as it exhibits the highest activity in the target process and demonstrates a high yield of 2-MF (81 %, 1 g of catalyst, 200 °C, 4 hours).

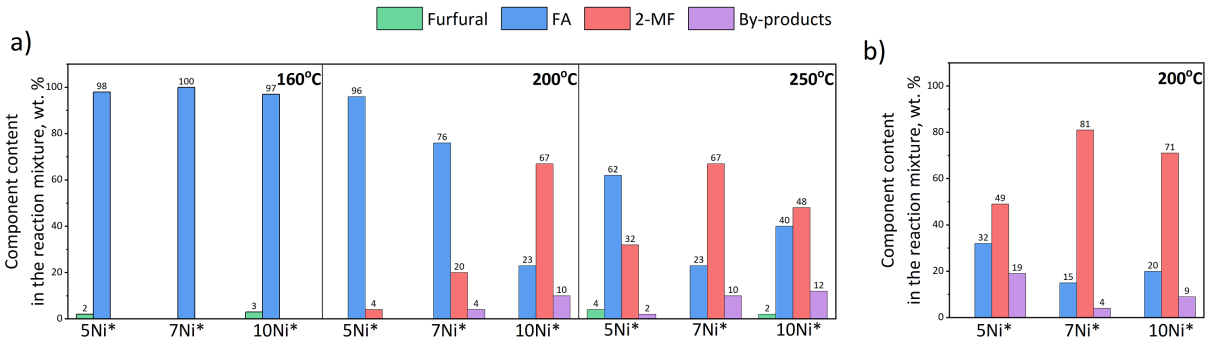

FIG. 5. The composition of the reaction mixture in the furfural hydroconversion over catalysts with different nickel contents. Reaction conditions: batch reactor, $P(H_2) = 5$ MPa, V(furfural) $= 4.8$ ml, V(i-PrOH) $= 55.2$ ml, $t = 4$ h, a) $m_{cat} = 0.3$ g; b) $m_{cat} = 1.0$ g; * by-products – 2-MTHF, THFA

3.3. Study of the 7Ni catalyst morphology and phase composition by HRTEM and XRD in situ methods

We used high-resolution transmission electron microscopy (HRTEM) and in situ X-ray diffraction (XRD) methods for a detailed study of the surface morphology and phase composition of the reduced 7Ni catalyst.

Figure 6 shows the in-situ X-ray diffraction patterns of the catalyst during stepwise reduction. In the temperature range of 30 – 175 °C, we do not observe any changes in the diffraction pattern. At a temperature of 200 °C, intense reflections of Cu appear at $2\theta = 43.2°$ and $50.3°$.

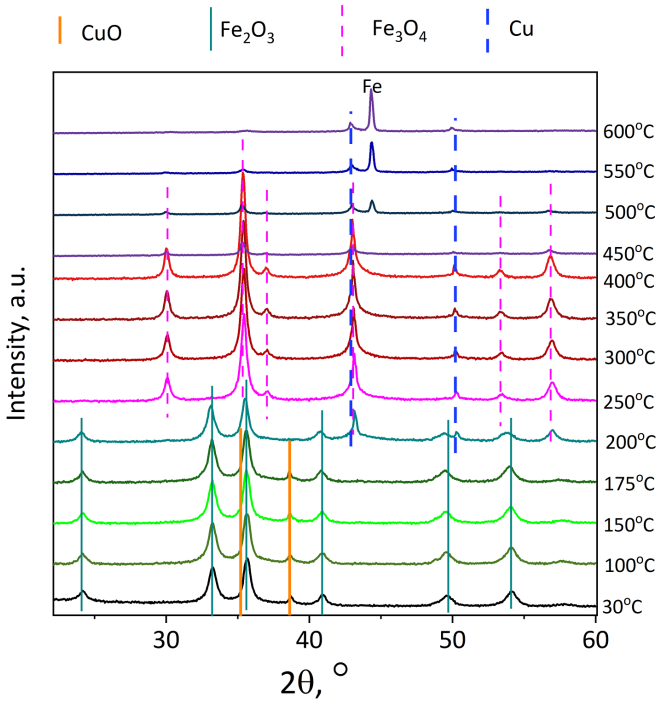

FIG. 6. In situ H_2 XRD patterns for the 7Ni catalyst

With a further increase in temperature to 250 °C, the reflections of CuO and Fe_2O_3 disappear. Peaks corresponding to reflections of iron oxide Fe_3O_4 and metallic copper appear. When the reduction temperature reaches 450 °C, there is a significant decrease in the intensity of the Fe_3O_4 reflections and a reduction in the corresponding lattice parameter (from 8.38 to 8.21 Å). Presumably, it is observed due to aluminum being incorporated into the lattice of iron oxide. The spinel Fe_2AlO_4 forms, and a narrow peak appears at 44.6°, corresponding to the metallic iron reflection. The diffraction pattern at 550 – 600 °C predominantly shows reflections from Cu and Fe.

Based on the HRTEM data for the 7Ni catalyst reduced at 250 °C and passivated with ethyl alcohol, we can identify several structural features of this sample. Copper is represented by a metallic phase (10 – 50 nm) covered with an oxide layer (Fig. 7b). Aluminum and iron exist in the form of individual oxide phases (Fig. 7a), sized 2 – 3 nm and 10 – 20 nm, respectively; these oxides create a matrix over which the copper and nickel phases are distributed. Nickel is primarily represented by an oxide phase, sized 2 – 3 nm, distributed over the surface of the iron and aluminum oxides (Fig. 7b). Additionally, nickel forms a core-shell structure with copper, where the core is nickel oxide, and the shell is copper oxide; the total size of such particles varies from 3 to 5 nm (Fig. 7c).

Summarizing the data obtained for the 7Ni catalyst in both oxidized and reduced forms, we can draw a conclusion about its phase composition and morphology. The fresh sample contains individual oxide phases of all metals. During reduction (250 °C), copper is completely converted into a metallic form, while nickel is partially reduced to metal, and iron and aluminum remain in oxide form (Fe_3O_4 and Al_2O_3, respectively). Based on the obtained data, we assume that the active component of the 7Ni catalyst is represented by finely dispersed metal particles of copper and nickel.

3.4. Study of spent 7Ni catalyst

At relatively high temperatures and due to the high activity of the catalyst, furfural and its hydroconversion products can polymerize on the catalyst surface, resulting in the formation of polymer structures that deactivate the active sites.

To confirm the theory of catalyst deactivation during the reaction, a complex of physicochemical methods was used to examine the spent 7Ni sample. The HRTEM results indicate that carbonization occurs on the catalyst surface. Mostly, amorphous carbon is located on the particles of iron and aluminum oxide, forming filament-like structures with a metal-containing center (Fig. 8a). Additionally, carbon is adsorbed on the catalyst surface, leading to its gradual deactivation (Fig. 8b–c). The average particle size of the catalyst does not significantly increase, indicating that dispersity is preserved

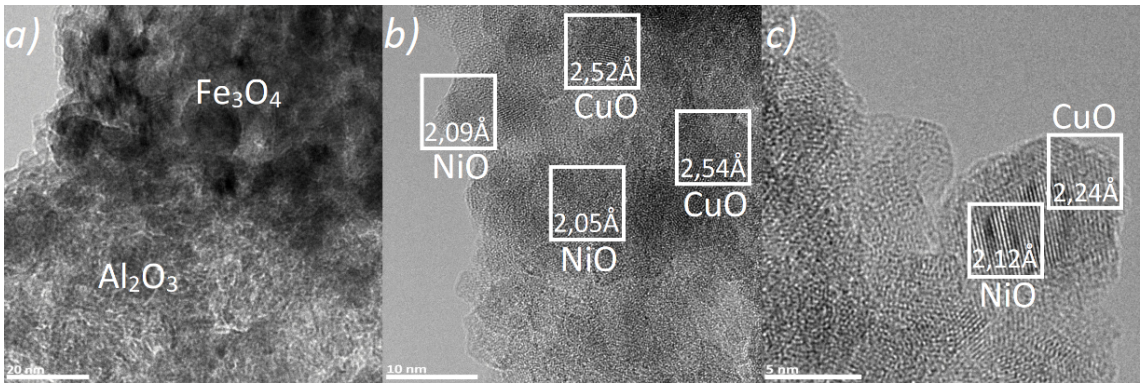

FIG. 7. HRTEM images: a) phases of hematite and aluminum oxide; b) individual phases of copper oxide (2.52, 2.54 Å are the interplanar distances corresponding to the [002] and [−111] reflections, respectively) and nickel oxide (2.05, 2.09 Å are the interplanar distances corresponding to the [200] reflection); c) NiCu-O core-shell structure (2.12, 2.24 Å – interplanar distances corresponding to reflections [200] of NiO and [200] of CuO, respectively)

during the reaction. On the surface of the spent sample, all metals are present in their oxide forms: Cu_2O, NiO, Fe_3O_4, and Al_2O_3 (Fig. 8d).

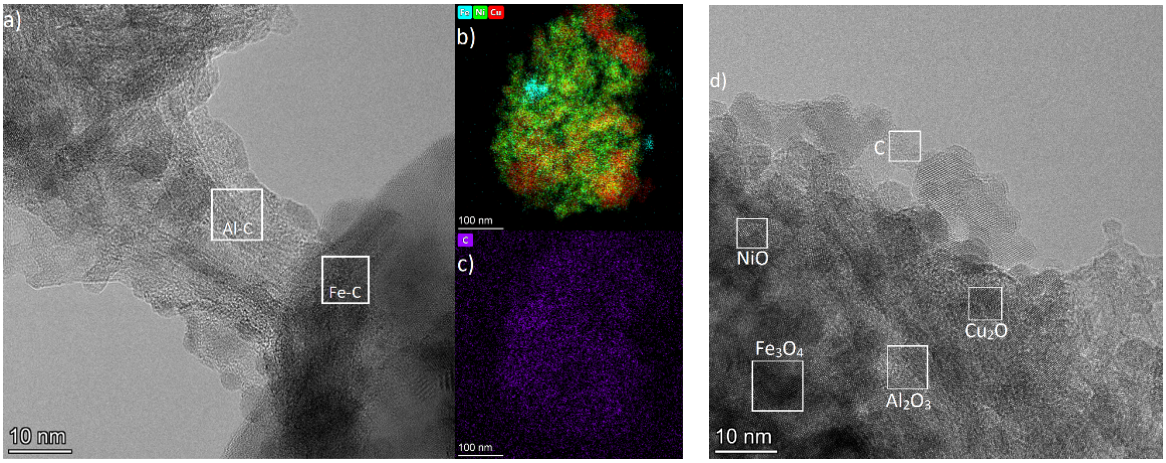

FIG. 8. a) HRTEM image of filament-like C–Al and Fe–Al structures; mapped HRTEM images for b) iron, copper, nickel; c) carbon; d) HRTEM image of nickel, copper, aluminum, ferric oxide, and amorphous carbon

CHNS analysis of the spent 7Ni catalyst sample showed that the mass content of carbon in the catalyst reaches 4.7 wt.%.

A spent sample of the 7Ni catalyst was studied using thermal analysis (Fig. 9) to determine the content of adsorbed water and organic compounds. The TG curve indicates that mass loss of the sample occurs in four steps. Analyzing the DTG curve, the temperatures at which changes in the rate of weight loss occur were identified. The maximum values on the DTG are illustrated by extremum points. The first extremum is detected at approximately 99 °C, which corresponds to the evaporation of adsorbed water (4.4 wt.%). Additionally, two more regions of mass loss are observed at 239 °C (2.6 wt.%) and 435 °C (0.9 wt.%), where reagents and products from two different groups of active sites of the catalyst are likely desorbed. With a further increase in temperature, high-molecular compounds (0.7 wt.%) evaporate.

Based on the data obtained for the spent 7Ni catalyst, we can draw conclusions about the nature of deactivation in such systems. During the reaction, products and reagents are adsorbed on the surface of active centers, leading to their polymerization and the formation of high-molecular compounds. To reduce the amount of carbon deposits on the catalyst surface and prevent its deactivation, it is necessary to either increase the hydrogen pressure in the system or to preliminarily purify the raw material before the experiment (furfural is prone to polymerization during long-term storage). These methods for reducing carbonaceous deposits are widely used in industry for hydroconversion processes involving furfural. Additionally, the catalyst can be regenerated after the reaction in a stream of hydrogen at the reduction temperature. For example, in the work [42], a copper-zinc catalyst was studied during the hydroconversion of furfural in a batch reactor. The catalyst maintains its activity over 6 cycles of reaction and regeneration.

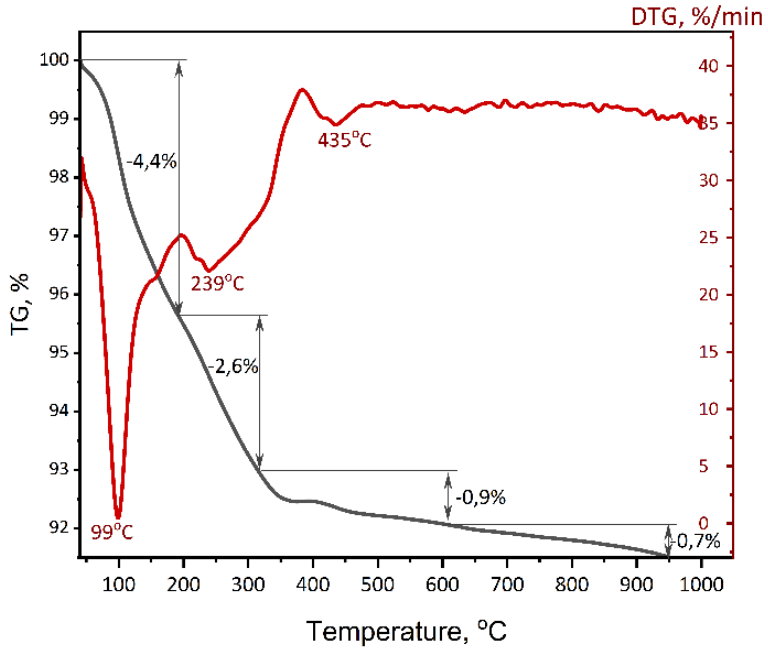

FIG. 9. TG and DTG curves for the spent 7Ni catalyst

3.5. Testing the selected catalyst in a flow type reactor

To understand how the selected 7Ni catalyst will behave under near-industrial conditions, we conducted a series of experiments in a flow-type reactor. The reaction conditions were established based on experiments conducted in a batch reactor (flow reactor, $P(H_2) = 5.0$ MPa, $T = 200$ °C, $m_{\text{cat}} = 1.0$ g, catalyst fraction = 0.25 – 0.50 mm, catalyst:quartz = 1 : 4 (vol.)). By varying the liquid hourly space velocity (LHSV, 1 – 8 h^{-1}), we obtained different ratios of products; however, the conversion of furfural and selectivity to 2-MF were identified as the most important parameters (Fig. 10).

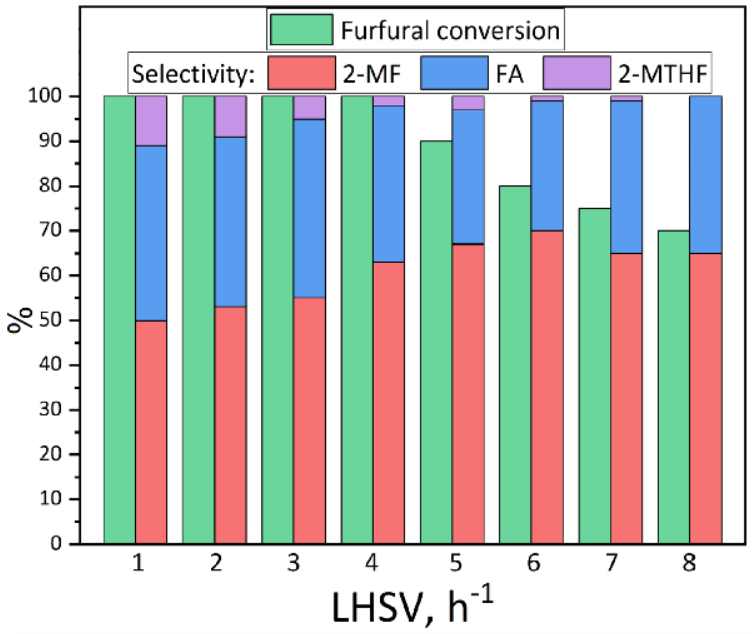

FIG. 10. Diagram of dependencies of furfural conversion and product selectivity on LHSV. Reaction conditions: flow reactor, $P(H_2) = 5.0$ MPa, $T = 200$ ° C, $m_{\text{cat}} = 1.0$ g, catalyst fraction = 0.25 – 0.50 mm, catalyst:quartz = 1 : 4 (vol.)

Based on the data obtained for furfural conversion and 2-MF selectivity, we chose a deliberately high LHSV value (6 h^{-1}), which allows for a faster evaluation of catalyst performance under severe conditions. Regarding the lower LHSV

values in the range of 1 to 4, there is a complete furfural conversion but low selectivity for 2-MF. It is due to the reaction of furan ring hydrogenation, resulting in the formation of 2-MTHF and THFA. At higher LHSV values, the conversion of furfural decreases significantly due to a reduction in contact time. Thus, we obtained the dependence of furfural conversion and 2-MF selectivity on the reaction time at LHSV $= 6$ h^{-1}. During the first 4 hours of the reaction in flow mode, the catalyst retains its activity (furfural conversion of 80 – 90 %, selectivity for 2-MF of 75 – 80 %). However, after 4 hours, there is a decrease in selectivity to 60 – 65 %, while maintaining furfural conversion.

As a result, it can be noted that the activity of the 7Ni catalyst does not fall over time, and furfural conversion is maintained at 80 – 90 % for 5 hours. During the reaction, there is a trend toward a decrease in selectivity for 2-MF; however, selectivity for FA rises (Fig. 11). It is possible that during the reaction, the nickel centers, on which hydroconversion to 2-MF partially depends, become deactivated [7,43]. Copper centers may also become deactivated, but their quantity is higher than that of nickel centers due to the higher copper content in the catalyst. Thus, by choosing the optimal reaction conditions over this catalyst, it is possible to achieve a high yield of both FA and 2-MF.

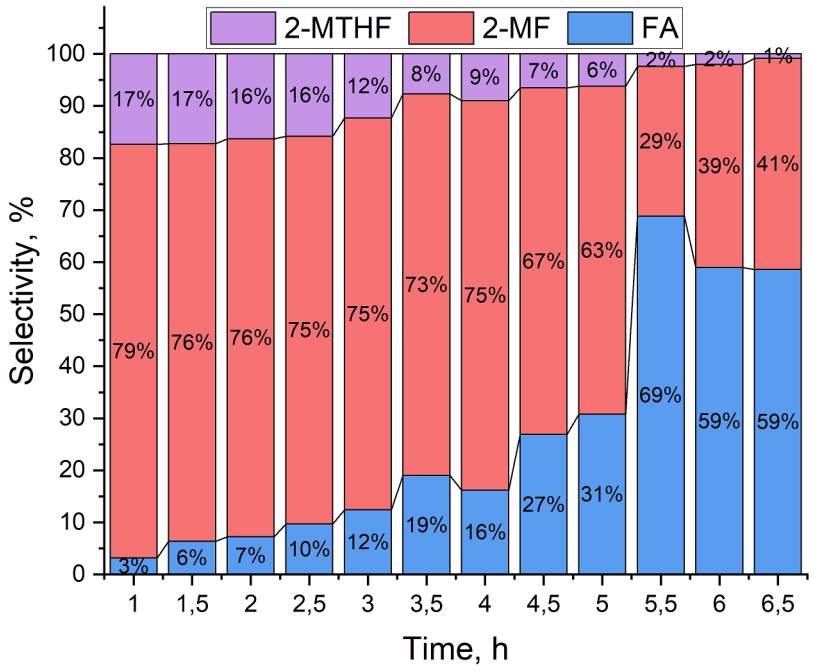

FIG. 11. Diagram of dependencies 2-MF, FA, and 2-MTHF selectivity on time. Reaction conditions: flow reactor, LHSV $= 6$ h^{-1}, $P(H_2) = 5.0$ MPa, $T = 200$ °C, $m_{\text{cat}} = 1.0$ g, catalyst fraction $= 0.25$ – 0.50 mm, catalyst:quartz $= 1 : 4$ (vol.)

The work [44] also studied the gas-phase hydroconversion of furfural in a flow reactor over copper-zinc catalysts. The reaction was carried out in the gas phase at a temperature of 200 °C, and as a result, the yield of 2-MF reached 95 % with 100 % conversion of furfural. Due to the lower LHSV (1.5 h^{-1}) compared to our work, the catalyst retained its activity after 10 hours of reaction. This process was also studied in liquid phase mode in work [45]. Hydroconversion of furfural took place at 180 °C and elevated hydrogen pressure (1 MPa) over a cobalt-containing catalyst. As a result, the conversion of furfural was 100 %, and the yield of 2-MF was 94 %, with a relatively low value of LHSV $= 0.5$ h^{-1} (calculated from the approximation that the bulk density of the catalyst is 1 g/cm^3).

Thus, the advantage of our method lies in higher LHSV values and, consequently, higher productivity. However, the service life of the catalyst is reduced due to carbonization of the active sites. Possible ways to reduce the carbonization of the catalyst include increasing the flow rate and pressure of hydrogen [46], as well as prepurifying the feedstock used in furfural refineries.

4. Conclusions

New NiCu-containing catalysts with different nickel oxide contents were prepared by the alloy method for furfural hydroconversion to 2-MF and FA. As a result of testing the obtained systems in a batch reactor in the target process, the 7Ni19Cu61Fe13Al (7Ni) catalyst was chosen as the most active. 100 % conversion of furfural and 81 % yield of 2-MF are achieved over 7Ni catalyst.

Analysis of the most active 7Ni catalyst by a complex of physicochemical methods showed that the fresh sample contains individual oxide phases of all metals. When this catalyst is reduced (250 °C), copper is completely converted into a metallic form, nickel is partially reduced to metal, and iron and aluminum are oxides (Fe_3O_4 and Al_2O_3, respectively).

The active component of the catalyst is represented by metallic copper (10 – 50 nm) and nickel (3 – 5 nm), which do not form joint phases. During the reaction, the catalyst is deactivated due to the irreversible sorption of reagents and reaction products on the surface, as well as their polymerization on the catalyst active sites. The total carbon content after the reaction in a batch reactor was 4.7 wt.%.

The selected 7Ni catalyst was tested in a flow reactor in solvent-free furfural hydroconversion. We have shown the possibility of obtaining 2-MF with a selectivity of 75 – 80 % at 80 – 90 % furfural conversion for 4 hours. After that, the trend in selectivity changes: for FA it rises to 55 – 60 %, and for 2-MF it decreases to 35 – 40 % while maintaining the furfural conversion. Compared to other catalysts used in this process, 7Ni demonstrates good results at a higher LHSV, and therefore has higher productivity.

References

[1] Dietrich K., Dumont M.-J., Del Rio L.F., Orsat V. Producing PHAs in the Bioeconomy – Towards a Sustainable Bioplastic. *Sustainable Production and Consumption*, 2017, **9**, P. 58–70.

[2] Nhien L.C., Long N.V.D., Lee M. Novel hybrid reactive distillation with extraction and distillation processes for furfural production from an actual xylose solution. *Energies*, 2021, **14** (4), 1152.

[3] Xu C., Paone E., Rodríguez-Padrón D., Luque R., Mauriello F. Recent Catalytic Routes for the Preparation and the Upgrading of Biomass Derived Furfural and 5-Hydroxymethylfurfural. *Chemical Society Reviews*, 2020, **49** (13), P. 4273–4306.

[4] Zhang X., Xu S., Li Q., Zhou G., Xia H. Recent advances in the conversion of furfural into bio-chemicals through chemo-and bio-catalysis. *RSC advances*, 2021, **11** (43), P. 27042–27058.

[5] Wang Y., Zhao D., Rodríguez-Padrón D., Len C. Recent Advances in Catalytic Hydrogenation of Furfural. *Catalysts*, 2019, **9** (10), 796.

[6] Li S., Li N., Li G., Wang A., Cong Y., Wang X., Zhang T. Synthesis of Diesel Range Alkanes with 2-Methylfuran and Mesityl Oxide from Lignocellulose. *Catalysis Today*, 2014, **234**, P. 91–99.

[7] Sitthisa S., Sooknoi T., Ma Y., Balbuena P.B., Resasco D.E. Kinetics and Mechanism of Hydrogenation of Furfural on Cu/SiO_2 Catalysts. *J. of Catalysis*, 2011, **277** (1), P. 1–13.

[8] Srivastava S., Jadeja G.C., Parikh J. Copper-Cobalt Catalyzed Liquid Phase Hydrogenation of Furfural to 2-Methylfuran: An Optimization, Kinetics and Reaction Mechanism Study. *Chemical Engineering Research and Design*, 2018, **132**, P. 313–324.

[9] Seo G. Hydrogenation of Furfural over Copper-Containing Catalysts. *J. of Catalysis*, 1981, **67** (2), P. 424–429.

[10] Dutta S., De S., Saha B., Alam M.I. Advances in conversion of hemicellulosic biomass to furfural and upgrading to biofuels. *Catalysis Science & Technology*, 2012, **2** (10), P. 2025–2036.

[11] Šivec R., Huš M., Likozar B., Grilc M. Furfural Hydrogenation over Cu, Ni, Pd, Pt, Re, Rh and Ru Catalysts: Ab Initio Modelling of Adsorption, Desorption and Reaction Micro-Kinetics. *Chemical Engineering J.*, 2022, **436**, 135070.

[12] Wang Z., Wang X., Zhang C., Arai M., Zhou L., Zhao F. Selective Hydrogenation of Furfural to Furfuryl Alcohol over Pd/TiH_2 Catalyst. *Molecular Catalysis*, 2021, **508**, 111599.

[13] Dong F., Zhu Y., Zheng H., Zhu Y., Li X., Li Y. Cr-free Cu-catalysts for the selective hydrogenation of biomass-derived furfural to 2-methylfuran: The synergistic effect of metal and acid sites. *J. of Molecular Catalysis A: Chemical*, 2015, **398**, P. 140–148.

[14] Wang S., Zhao G., Lan T., Ma Z., Wang H., Liu Y., Lu Y. Gas-phase hydrogenation of furfural to furfuryl alcohol: A promising Cu/SiO_2 catalyst derived from lamellar Cu-based hydroxy double salt. *Fuel*, 2024, **372**, 132095.

[15] Tyuryaeva I.Ya., Chistyakova G.A. *Catalysts for basic organic synthesis*, GIPH 68, Leningrad, 1967, 85.

[16] Chistyakova G.A., Zubritskaya N.G. Hydrogenation catalysts based on metal chromites. *GIPH collection*, 1973, **68**, P. 5–13.

[17] Demirbas A. Progress and Recent Trends in Biofuels. *Progress in Energy and Combustion Science*, 2007, **33** (1), P. 1–18.

[18] Zhao Y., Tao L. Towards catalytic reactions of Cu single-atom catalysts: Recent progress and future perspective. *Chinese Chemical Letters*, 2024, **35** (2), 108571.

[19] Selishcheva S., Sumina A., Gerasimov E., Selishchev D., Yakovlev V. High-Loaded Copper-Containing Sol-Gel Catalysts for Furfural Hydroconversion. *Int. J. of Molecular Sciences*, 2023, **24** (8), 7547.

[20] Yao Y., Yu Z., Lu C., Sun F., Wang Y., Sun Z., Wang A. Highly efficient Cu-based catalysts for selective hydrogenation of furfural: A key role of copper carbide. *Renewable Energy*, 2022, **197**, P. 69–78.

[21] Şebin M.E., Akmaz S., Koc S.N. Hydrogenation of Furfural to Furfuryl Alcohol over Efficient Sol-Gel Nickel-Copper/Zirconia Catalyst. *J. of Chemical Sciences*, 2020, **132** (1), 157.

[22] Akmaz S., Algorabi S., Koc S.N. Furfural Hydrogenation to 2-methylfuran over Efficient Sol-gel Copper-cobalt/Zirconia Catalyst. *The Canadian J. of Chemical Engineering*, 2021, **99** (S1), S562–S574.

[23] Kalong M., Hongmanorom P., Ratchahat S., Koo-amornpattana W., Faungnawakij K., Assabumrungrat S., Srifa A., Kawi S. Hydrogen-Free Hydrogenation of Furfural to Furfuryl Alcohol and 2-Methylfuran over Ni and Co-Promoted $Cu/\gamma\text{-}Al_2O_3$ Catalysts. *Fuel Processing Technology*, 2021, **214**, 106721.

[24] Wang Y., Hu D., Guo R., Deng H., Amer M., Zhao Z., Xu H., Yan K. Facile Synthesis of Ni/Fe_3O_4 Derived from Layered Double Hydroxides with High Performance in the Selective Hydrogenation of Benzaldehyde and Furfural. *Molecular Catalysis*, 2022, **528**, 112505.

[25] Rajabi F., Arancon R.A.D., Luque R. Oxidative Esterification of Alcohols and Aldehydes Using Supported Iron Oxide Nanoparticle Catalysts. *Catalysis Communications*, 2015, **59**, P. 101–103.

[26] Wang C., Zhang J., Gao X., Zhao T. Research Progress on Iron-Based Catalysts for CO_2 Hydrogenation to Long-Chain Linear α-Olefins. *J. of Fuel Chemistry and Technology*, 2023, **51** (1), P. 67–85.

[27] Sunyol C., Owen R.E., González M.D., Salagre P., Cesteros Y. Catalytic hydrogenation of furfural to tetrahydrofurfuryl alcohol using competitive nickel catalysts supported on mesoporous clays. *Applied Catalysis A: General*, 2021, **611**, 117903.

[28] Li Z., Zhu M., Chen X., Mei H. Catalytic performance of Ni/Al_2O_3 catalyst for hydrogenation of 2-methylfuran to 2-methyltetrahydrofuran. *J. of Fuel Chemistry and Technology*, 2018, **46** (1), P. 54–58.

[29] Xu C., Paone E., Rodríguez-Padrón D., Luque R., Mauriello F. Recent Catalytic Routes for the Preparation and the Upgrading of Biomass Derived Furfural and 5-Hydroxymethylfurfural. *Chemical Society Reviews*, 2020, **49** (13), P. 4273–4306.

[30] Selishcheva S.A., Smirnov A.A., Fedorov A.V., Bulavchenko O.A., Saraev A.A., Lebedev M.Yu., Yakovlev V.A. Highly Active CuFeAl-Containing Catalysts for Selective Hydrogenation of Furfural to Furfuryl Alcohol. *Catalysts*, 2019, **9** (10), 816.

[31] Yakovlev V.A., Khromova S.A., Sherstyuk O.V., Dundich V.O., Ermakov D.Yu., Novopashina V.M., Lebedev M.Yu., Bulavchenko O.A., Parmon V.N. Development of New Catalytic Systems for Upgraded Bio-Fuels Production from Bio-Crude-Oil and Biodiesel. *Catalysis Today*, 2009, **144** (3–4), P. 362–366.
[32] Khromova S.A., Smirnov A.A., Bulavchenko O.A., Saraev A.A., Kaichev V.V., Reshetnikov S.I., Yakovlev V.A. Anisole Hydrodeoxygenation over Ni–Cu Bimetallic Catalysts: The Effect of Ni/Cu Ratio on Selectivity. *Applied Catalysis A: General*, 2014, **470**, P. 261–270.
[33] Selishcheva S.A., Lebedev D.Yu., Reshetnikov S.I., Trusov L.I., Yakovlev V.A. Kinetics of the Hydrotreatment of Rapeseed Oil Fatty Acid Triglycerides under Mild Conditions. *Catalysis in Industry*, 2014, **6** (1), P. 60–66.
[34] Alders D., Voogt F.C., Hibma T., Sawatzky G.A. Nonlocal screening effects in 2p X-ray photoemission spectroscopy of NiO (100). *Physical Review B*, 1996, **54** (11), 7716.
[35] Van Veenendaal M.A., Sawatzky G.A. Nonlocal screening effects in 2p X-ray photoemission spectroscopy core-level line shapes of transition metal compounds. *Physical Review Letters*, 1993, **70** (16), 2459.
[36] Batista J., Pintar A., Mandrino D., Jenko M., Martin V. XPS and TPR examinations of γ-alumina-supported Pd-Cu catalysts. *Applied Catalysis A: General*, 2001, **206** (1), P. 113–124.
[37] Bukhtiyarov V.I., Kaichev V.V., Prosvirin I.P. X-ray photoelectron spectroscopy as a tool for in-situ study of the mechanisms of heterogeneous catalytic reactions. *Topics in Catalysis*, 2005, **32**, P. 3–15.
[38] McIntyre N.S., Cook M.G. X-ray photoelectron studies on some oxides and hydroxides of cobalt, nickel, and copper. *Analytical chemistry*, 1975, **47** (13), P. 2208–2213.
[39] Descostes M., Mercier F., Thromat N., Beaucaire C., Gautier-Soyer M. Use of XPS in the determination of chemical environment and oxidation state of iron and sulfur samples: constitution of a data basis in binding energies for Fe and S reference compounds and applications to the evidence of surface species of an oxidized pyrite in a carbonate medium. *Applied Surface Science*, 2000, **165** (4), P. 288–302.
[40] Tan B.J., Klabunde K.J., Sherwood P.M. X-ray photoelectron spectroscopy studies of solvated metal atom dispersed catalysts. Monometallic iron and bimetallic iron-cobalt particles on alumina. *Chemistry of Materials*, 1990, **2** (2), P. 186–191.
[41] Fairley N., Carrick A., Fairley N. *Recipes for XPS Data Processing*. The Casa cookbook. Acolyte Science, Knutsford, 2005.
[42] Niu H., Luo J., Li C., Wang B., Liang C. Transfer hydrogenation of biomass-derived furfural to 2-methylfuran over CuZnAl catalysts. *Industrial & Engineering Chemistry Research*, 2019, **58** (16), P. 6298–6308.
[43] Srivastava S., Jadeja G.C., Parikh J. Copper-Cobalt Catalyzed Liquid Phase Hydrogenation of Furfural to 2-Methylfuran: An Optimization, Kinetics and Reaction Mechanism Study. *Chemical Engineering Research and Design*, 2018, **132**, P. 313–324.
[44] Yang X., Xiang X., Chen H., Zheng H., Li Y. W., Zhu Y. Efficient Synthesis of Furfuryl Alcohol and 2-Methylfuran from Furfural over Mineral-Derived Cu/ZnO Catalysts. *ChemCatChem*, 2017, **9** (15), P. 3023–3030.
[45] Liu P., Sun L., Jia X., Zhang C., Zhang W., Song Y., Li C. Efficient one-pot conversion of furfural into 2-methyltetrahydrofuran using non-precious metal catalysts. *Molecular Catalysis*, 2020, **490**, 110951.
[46] Forzatti P., Lietti L. Catalyst deactivation. *Catalysis Today*, 1999, **52** (2-3), P. 165–181.

Submitted 25 April 2024; revised 16 October 2024; accepted 10 December 2024

Information about the authors:

Anastasiya A. Sumina – Federal Research Center Boreskov Institute of Catalysis SB RAS, Lavrentiev Ave. 5, Novosibirsk 630090, Russia; ORCID 0009-0006-4393-7866; sumina@catalysis.ru

Svetlana A. Selishcheva – Federal Research Center Boreskov Institute of Catalysis SB RAS, Lavrentiev Ave. 5, Novosibirsk 630090, Russia; ORCID 0000-0003-2768-9680; svetlana@catalysis.ru

Olga A. Bulavchenko – Federal Research Center Boreskov Institute of Catalysis SB RAS, Lavrentiev Ave. 5, Novosibirsk 630090, Russia; ORCID 0000-0001-5944-2629; obulavchenko@catalysis.ru

Vadim A. Yakovlev – Federal Research Center Boreskov Institute of Catalysis SB RAS, Lavrentiev Ave. 5, Novosibirsk 630090, Russia; ORCID 0000-0001-5015-3521; yakovlev@catalysis.ru

Conflict of interest: the authors declare no conflict of interest.